THE JOURNAL OF PHYSICAL CHEMISTRY B
A JOURNAL OF THE AMERICAN CHEMICAL SOCIETY

pubs.acs.org/JPCB

Article

Effect of the Molecular Weight of Polyelectrolyte and Surfactant Chain Length on the Solid-Phase Molecular Self-Assembly

Published as part of The Journal of Physical Chemistry B virtual special issue "Women Scientists in China".

Xiangyu Dou,[§] Shuitao Gao,[§] Zekang Lu, Jianbin Huang, and Yun Yan*

Cite This: https://doi.org/10.1021/acs.jpcb.3c07071

ABSTRACT: Solid-phase molecular self-assembly (SPMSA) is emerging as an efficient approach, leading to scale-span self-assembled supramolecular films. With SPMSA, freestanding macroscopic supramolecular films can be formed upon mechanically pressing the precipitates formed with polyelectrolytes and oppositely charged surfactants. Herein, we report that the film formation ability and the mechanical strength of the resultant film depend highly on the surfactant chain lengths and the molecular weight of polyelectrolytes. A coarse-grained molecular dynamics study revealed that the longer surfactant chains are beneficial for the ordered assembly of surfactant bilayers in the film, whereas the larger molecular weight of PE favors the enhanced mechanical strength of the film by promoting the long-range order of the surfactant bilayers. The current results disclosed the physical insight of the surfactant chain length and the molecular weight of polyelectrolytes into the film structure and mechanical strength, which is of practical importance in guiding the creation of SPMSA materials.

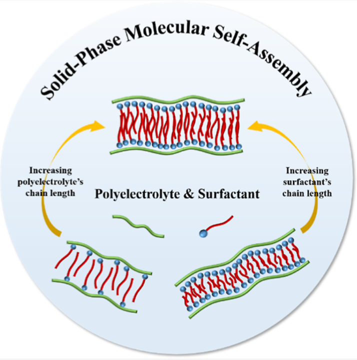

1. INTRODUCTION

Molecular self-assembly represents an effective bottom-up approach for designing structural materials with emergent functionalities.[1,2] It is a process in which molecules assemble into ordered structures with unique properties.[3] Advanced intelligent materials, such as sensors,[4] photoelectric conversion devices,[5] biomedical devices,[6] luminescent materials,[7] and so forth, can be obtained by molecular self-assembly.[8] Typically, these materials are prepared in the form of suspensions in solution.[9−13] Apart from conventional slow deposition and evaporation-induced film formation,[14−18] few solution-based molecular self-assembly have demonstrated the capability of spanning multi-scales to create bulk macroscopic materials.[19] So far, it seems difficult to obtain continuous macroscopic materials from solution-based molecular self-assembly.[20]

In stark contrast, Nature epitomizes a remarkable proficiency in orchestrating multiscale self-assembly. A familiar example is the aggregation of particulate matter, exemplified by the clumping of milk powder particles, where diminutive crystalline entities coalesce to yield larger aggregates.[21] This process is underpinned by the pivotal role of water, which orchestrates the rearrangement of molecular constituents and serves as a bridging mediator between individual particles.[22]

Inspired by this phenomenon, recently, our group postulated the strategy of solid-phase molecular self-assembly (SPMSA),[23−34] which elegantly utilizes the caking tendency of particles in precipitates formed with molecules with self-assembly ability, in particular, precipitates formed with a surfactant and an oppositely charged polyelectrolyte (PE).[24] Under mild mechanical pressure and in the presence of physically adsorbed water to facilitate molecular rearrangement, the caking in the PE/surfactant precipitates leads to a self-supporting supramolecular film, where the surfactant bilayers were bridged by the PE chains to form continuous macroscopic structures. This not only allows the preparation of noncolloidal form self-supporting macroscopic molecular self-assembled materials but also makes it possible to get diversified functions.[23,24,26,28−30,32,33,35] However, we found that the film formation ability and the resultant mechanical strength of the film depend highly on the surfactant and polyelectrolyte structure, in particular, the surfactant chain length and the molecular weight of the PE. In order to reveal the physical insight behind this effect, herein, we report a systematic study of the films formed with sodium alkyl sulfates and poly dimethyl diallyl ammonium chloride (PDDA). Experimentally, we fabricated the SPMSA films by varying the surfactant chain length while keeping the molecular weight of PDDA unchanged and by fixing the surfactant chain length but varying the molecular weight of PDDA. The structure of the film and the mechanical strength of these films were studied, which reveals that the longer surfactant chains and higher

Received: October 25, 2023
Revised: November 29, 2023
Accepted: November 30, 2023

molecular weight of PDDA are favorable for film formation and the film's mechanical strength. Then, theoretically, the coarse-grained molecular dynamics (CG-MD) method was employed to reveal the role of surfactant chain length and molecular weight of PDDA on the film structure. It is found that the longer surfactant chain length favors the ordered assembly of the surfactant bilayers in the film, whereas the higher molecular weight is good for the formation of the long-range order of the surfactant bilayers. Thus, the combination of the experiments and CG-MD simulation provided a full view of the effect of the molecular structure on the structural and mechanical structure of the supramolecular film based on SPMSA, which is of practical guidance for the creation of functional supramolecular films in the near future.

2. METHOD

2.1. Experiments. *2.1.1. Materials.* Surfactants used in this work, sodium dodecyl sulfate (SDS), sodium decyl sulfate (SDeS), sodium octyl sulfate (SOS), and polydiallyldimethylammonium chloride (PDDA, 20 wt % in water, M_w = 200k; M_w = 350k; M_w = 500k) were obtained commercially from Aladdin and used without further purification. Other reagents were of AR grade and were purchased from Beijing Chemical Reagents Company. The aqueous solutions were prepared using Mili-Q water at 18 MΩ.

2.1.2. Methods. SPMSA of surfactants and PDDA: In order to obtain the precipitates composed of surfactants and PDDA, a 100 mM aqueous surfactant solution was added into the aqueous solution of PDDA. Then, the precipitates were collected and pressed by finger over a glass plate or loaded into a household noodle machine. A large-scale opaque plastic film was obtained immediately after pressing in both protocols, which became transparent within 30 min. The thickness of the film can be conveniently controlled between 0.1 and 5 mm by setting the distance between the two rollers of the noodle machine.

XRD measurements: X-ray diffraction (XRD) measurements were performed on a Rigaku D_{max}-2400 diffractometer with Cu Kα radiation. The solid samples were placed on clean glass slides for small-angle range tests. The lamellar period d in each sample was calculated using Bragg's Law, where $d = \lambda/2\sin\theta$.

FT-IR measurements: The Fourier transform infrared (FT-IR) measurements were carried out on a Nicolet iN10 MX microscopic infrared spectrometer (ThermoS-7 Scientific Co., USA) in the range of 4000−600 cm^{-1} under ambient conditions. The spectrometer was equipped with an attenuated total reflection accessory with a Smart iTR (diamond).

Mechanical tests: The mechanical properties of the films were tested using a UTM2503X electronic universal testing machine under an ambient environment. All of the mechanical tests were measured at least three times to rule out coincidences such as defects and bubbles produced during the film fabrication. The ambient humidity was about 50% unless otherwise specified in special instructions. The tensile speed was set to 5 mm·min^{-1}.

2.2. CG MD Simulation. *2.2.1. Overall Principle of Simulation.* Due to the multiscale nature of our SPMSA, we adhere to multiscale MD simulation, employing quantitatively corrected all-atom parameters along with all-atom corrected CG parameters, which is verified successful in explaining the role of water, mechanical pressure, and size of the preassembled nano domains in SPMSA in our previous work.[36] This work varies the chain length of only a specific molecular structure of sodium alkyl sulfate. For certain problems involving chemical bond fracture and electron transfer, ab initio simulation techniques are utilized, providing the full atomic partial charge for the entire system. Specifically, the quantum chemical computation was performed using the 1.14*CM1A-LBCC method[37] on Lipargen.[38]

The final computations are conducted on a coarse-grained scale. In order to accommodate the current complexity scale, the model adopts the latest version of Martini 3.0.[39] With the fractional charge model obtained, the all-atom optimized potentials for liquid simulations (OPLS-AA) force field[40,41] was used to study the specific molecular interaction in the current surfactant−PDDA system. Finally, the CG simulation parameters (Tables 1 and 2) were optimized using the OPLS-AA force field.[40] The Martini force field[42] with 1000 times higher calculation efficiency is employed rather than OPLS-AA simulation.[41]

Table 1. Charge States of Each Bead Type

molecule	type	charge/e
sodium alkyl sulfate	**C1**	−0.0105
	C1v	0.2437
	Q4n	−1.2227
PDDA-chain	**C2v**	0.1128
	Q2p	0.8872
water	**W**	0

Table 2. Van der Waals Interactions between Each Pair of Beads

pair-type		L-J-parameter	
		ε (kcal/mol)	σ/Å
C2v	C2v	0.7740	4.7
Q2p	Q2p	0.9508	4.7
C2v	Q2p	0.5551	6.2
C2v	Q4n	0.5727	5.2
C2v	C1	0.8815	4.7
C2v	C1v	0.8099	4.7
C2v	W	0.5781	4.65
C2v	TQ5	0.6271	5.11
Q2p	Q4n	1.0631	4.7
Q2p	C1	0.6013	4.85
Q2p	C1v	0.5344	6.2
Q2p	W	1.3047	4.65
Q2p	TQ5	1.1658	4.05
Q4n	Q4n	1.2423	4.7
C1	C1	0.8099	4.7
C1v	C1v	0.774	4.7
Q4n	C1	0.5191	5.7
Q4n	C1v	0.5478	5.2
Q4n	W	1.5335	4.65
Q4n	TQ5	1.5194	4.05
C1	C1v	0.8409	4.7
C1	W	0.4921	4.7
C1	TQ5	0.3788	5.24
C1v	W	0.5208	4.65
C1v	TQ5	0.3860	5.11
W	W	0.1111	4.7
W	TQ5	2.9393	3.75
TQ5	TQ5	0.2819	3.54

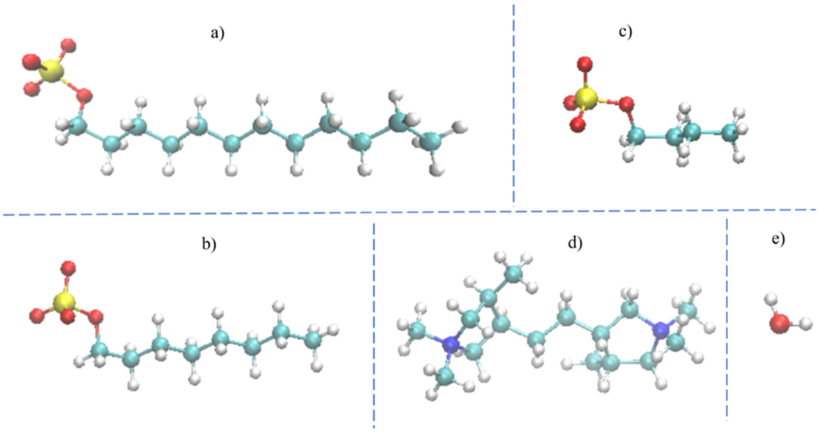

Figure 1. All-atom scenarios for the structure of surfactants of different chain lengths (a−c) and PDDA (d) and H_2O (e).

2.2.2. Details of the OPLS Force Field. The OPLS force field[43,44] comprises harmonic terms governing bond stretching and angle bending, along with Fourier series describing dihedral angles. Additionally, it incorporates Coulomb and Lennard-Jones interactions between atoms separated by three or more bonds, as presented in eq 1

$$\begin{aligned}E &= E_{\text{no-bond}} + E_{\text{bonds}} + E_{\text{angles}} + E_{\text{dihedral}}\\ &= \sum_i \sum_{j>i} \left[\frac{q_i q_j e^2}{r_{ij}} + 4\varepsilon_{ij}\left(\frac{\sigma_{ij}^{12}}{r_{ij}^{12}} - \frac{\sigma_{ij}^{6}}{r_{ij}^{6}}\right)\right] + \sum_{\text{bonds}} K_r(r - r_{\text{eq}})^2 +\\ &\quad \sum_{\text{angles}} K_\theta(\theta - \theta_{\text{eq}})^2 + \sum_i \left\{\frac{V_{1i}}{2}[1+\cos(\varphi_i)]\right.\\ &\quad + \frac{V_{2i}}{2}[1 - \cos(2\varphi_i)] + \frac{V_{3i}}{2}[1+\cos(3\varphi_i)]\\ &\quad \left. + \frac{V_{4i}}{2}[1 - \cos(4\varphi_i)]\right\}\end{aligned} \tag{1}$$

The total energy E of the system comprises distinct contributions from various energy terms, including Coulomb terms, Lennard-Jones terms, harmonic bond stretching terms, angle bending terms, and a Fourier series for torsional energetics. The partial atomic charge q is fixed at each atom's mass center, while i and j represent all pairs of atoms ($i < j$). The distance between atoms i and j is denoted by r_{ij}. Furthermore, ε_{ij} and σ_{ij} represent the potential well depth and Lennard-Jones radii, respectively.

The force constants K_r, K_θ, and V_{ni} (n = 1,2,3,4) are the force constants, which govern the strength of the harmonic bond stretching, angle bending, and Fourier series terms, respectively. Additionally, r_{eq}, θ_{eq}, and φ_i represent the equilibrium values for bond lengths, bond angles, and dihedral angles, respectively. These comprehensive energy terms capture the diverse interactions between atoms and provide a robust description of the system's molecular behavior.

The OPLS-AA model for the surfactant−PDDA-H_2O system is given in Figure 1. The models of three surfactant molecules with different chain lengths were shown, including molecules with 12, 8, and 4 carbons, shortened as SDS (Figure 1a), SOS (Figure 1b), and SBS (Figure 1c), respectively. The dimer of PDDA is shown in Figure 1d. The model of water is also given in Figure 1e since the SPMSA always contains a certain amount of physically adsorbed water.[36]

2.2.3. Martini Force Field. The Martini force field[39,42,45] is given in eq 2. The angle bending terms and the Fourier series for torsional energetics are ignored. So, the MD simulation based on the Martini force field is much faster than the AA force field.

$$\begin{aligned}E &= E_{\text{non-bond}} + E_{\text{bonds}}\\ &= \sum_i \sum_{j>i} \left[\frac{q_i q_j e^2}{r_{ij}} + 4\varepsilon_{ij}\left(\frac{\sigma_{ij}^{12}}{r_{ij}^{12}} - \frac{\sigma_{ij}^{6}}{r_{ij}^{6}}\right)\right] + \sum_{\text{bonds}} K_r(r - r_{\text{eq}})^2\end{aligned} \tag{2}$$

Martini 3.0 comprises seven chemical bead types: polar (P), intermediate/nonpolar (N), nonpolar (C), halogenated compounds (X), monovalent ions (Q), divalent ions (D), and water (W). All of the bead types come in three different sizes: standard (R-type beads, by default), small (S-beads, indicated with the prefix S), and tiny (T-beads, indicated with the prefix T).

X, D, and W are entirely novel chemical types that did not exist in previous versions. Except for the W and D beads, all of the beads possess subtypes, distinguished by numbers, indicating the relative polarity levels, ranging from 1 (low polarity) to a maximum value of 6 (high polarity). These subtypes allow for a more precise representation of the fundamental atomic structures, concerning chemical properties. Additional subtypes for specific chemical peculiarities can also be elaborated. Compared to previous versions, N and Q beads have undergone the most significant expansion to enhance the coverage of chemical space. From the perspective of partitioning between oil and water, N-type beads encompass the majority of the compounds, thereby providing more options to enable the development of accurate models. Figure 2 illustrates the coarse-grained scenarios for surfactants of different chain lengths and PDDA.

Tables 1 and 2 provide the charged states and intermolecular interactions for the system, respectively, and the precise calculations based on the Martini 3.0 force field rules are obtained for each bead type and bead pair within the multiscale MD simulation platform.

For the internal parameters of the PDDA molecule, specific information from relevant literature was referenced,[46] resulting in the interaction parameters for the PDDA molecule, as presented in Table 3. With this, a complete multiscale analysis and MD simulation platform for the ternary complex system is established.

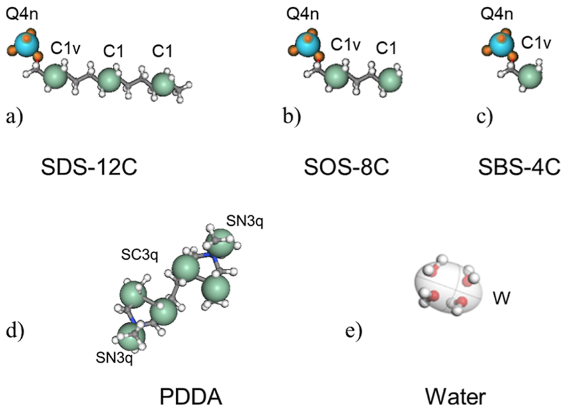

Figure 2. Martini 3.0 coarse-grained configurations of the PDDA−surfactant-H_2O system. Different alkyl sulfate groups with varying alkyl carbon chain lengths: (a) for SDS; (b) for SOS; (c) for SBS. The last two kinds of molecule are given (d) for the PDDA dimer and (e) for water.

Table 3. Internal Interactions of the PDDA Molecule

bond stretching	r_0 (Å)	k_r (kcal/mol)
SC3q-SC3q(intermonomer)	3.8626	298.6
SC3q-SC3q(in-circle)	2.2948	
SC3q-SN3q(in-circle)	2.9948	
	$E = k\theta(\cos\theta\text{-}\cos\theta_0)^2$	
bond bending	θ_0 (degrees)	k_θ (kcal/mol)
SC3q-SC3q-SC3q	99.25	11.945

3. RESULTS AND DISCUSSION

3.1. Experimental Results of SPMSA Formed with Sodium Alkyl Sulfates and PDDA. First of all, we test the ability of constructing SPMSA films with sodium alkyl sulfate of different chain lengths and the cationically charged polyelectrolyte PDDA of 500k. Both sodium dodecyl sulfate (SDS-C12) and sodium decyl sulfate (SDeS-C10) can form large amount of precipitates with PDDA (Figure 3a,b), whereas as the alkyl chain length is shortened to C8, namely, sodium octyl sulfate (SOS-C8), there are hardly any precipitates. The SDS-PDDA precipitates are nonsticky (Figure 3c), which can be further pressed into freestanding transparent films (Figure 3d,e). In contrast, the SDeS-PDDA precipitates are very sticky (Figure 3f,g), which can be pressed into transparent films (Figure 3h) only after drying for 10 min at 90 °C.

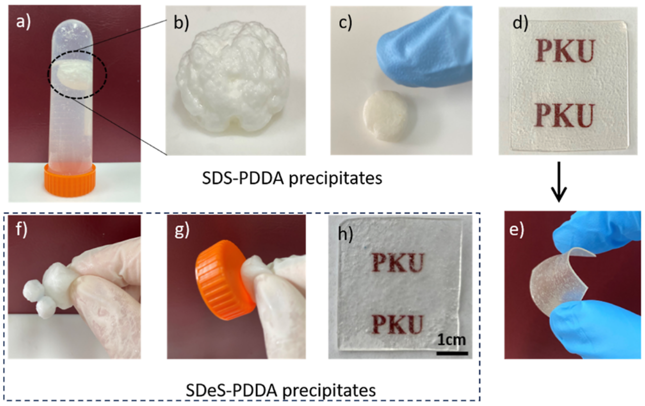

Figure 3. Preparation of the SPMSA films with sodium alkyl sulfates and PDDA. (a−e) Scenarios in the creation of SDS-PDDA films. (f−h) Scenarios in the creation of SDeS-PDDA films. The starting surfactant solutions are both 100 mM, and the 500k PDDA aqueous solution are 20%. Precipitates are formed at a charge balancing molar ratio for both systems, and the films are obtained from pressing the precipitates.

XRD measurements indicated the formation of surfactant bilayers in both films (Figure 4a), which are featured by the occurrence of similar 100 and diffraction peaks manifesting the distance of 3.4 and 3.0 nm, for the SDS-PDDA and SDeS-PDDA films, respectively. These distances are about 2 times of the increasing length of the corresponding surfactants (SDS ≈ 1.7 nm, SDeS ≈ 1.5 nm). FT-IR measurements (Figure 4b) revealed that the symmetric and asymmetric vibration band for the alkyl chains in the PDDA-SDS and PDDA-SDeS films occurred at 2852, 2922, and 2854, 2924 cm^{-1}, respectively, manifesting the alkyl chains packed less orderly as it becomes shorter.[29,47]

Next, the effect of the molecular weight of PDDA on film formation was examined. It was found that as the molecular weight of PDDA varies from 200 to 500k, similar precipitates would occur when they were mixed with SDS in solution. XRD measurements revealed that the diffraction peaks shifted to higher angles upon increasing the molecular weight of PDDA from 200k to 500k, and the thickness of bilayers decreased from 3.7 to 3.4 nm (Figure 5a). In the meantime, the symmetric and asymmetric vibration bands of SDS gradually shifted from 2854, 2923 to 2852, 2922 cm^{-1} in the FT-IR spectra (Figure 5b), indicating that the large molecular weight of PDDA facilitates the denser packing of SDS. This is understandable. The longer PDDA chains may seize more SDS molecules around their backbone, so that the local concentration of SDS can be enhanced, which favors the denser packing of SDS. Indeed, the interlayer distances in self-assembled systems would decrease with increasing concentration, which have been widely reported in previous studies[48,49] In line with the denser molecular packing facilitated by the long PDDA chains, the mechanical strength (Figure 5c) of the corresponding film is the largest (2.3 MPa) but with the smallest breaking strain (150%). In contrast, the looser molecular packing caused by the short PDDA chains would offer weaker film strength (1.6 and 1.2 MPa for the PDDA 350k and 200k, respectively) but larger breaking strain (185 and 240%). This means that the longer PE chains would form more robust bridges than the shorter ones between surfactant bilayers, thus offering stronger mechanical strength for the film.

3.2. Simulation of the Molecular Structure on the SPMSA Formation with an Optimized Martini Force Field. In order to disclose the physical insights behind the above experimental phenomena, we next used CG-MD to study the effect of the surfactant chain length and molecular weight of PDDA on the SPMSA film formation. Because four atoms were used to form one bead in the coarse-grained model, the alkyl chain lengths studied in the CG-simulation were set as 12C, 8C, and 4C, respectively. All the simulations were conducted with periodic boundary conditions, and all the three box dimensions are 6 nm × 180 nm × 9 nm. The coarse-grained molecular structures of different alkyl sulfate groups for CG-MD simulations are shown in Figure 2a−c, and their specific parameters are listed in Tables 1−3.

In Martini 3.0, the water molecule model is represented by a specific model called “W” (Figure 2e). Additionally, the

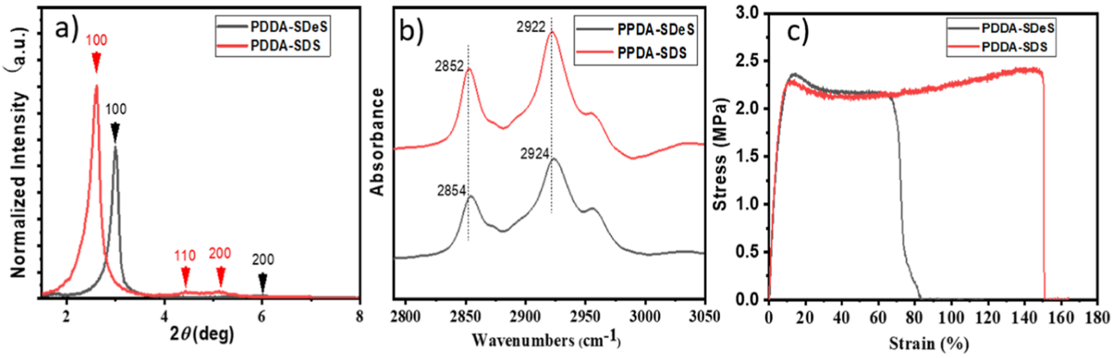

Figure 4. Effect of the surfactant chain longitude on the structure and property of the surfactant-PDDA films. (a) XRD patterns for the PDDA-SDS and PDDA-SDeS films. (b) FT-IR spectra for the PDDA-SDS and PDDA-SDeS films. (c) Mechanical test for the PDDA–surfactant films formed with PDDA and the surfactant of different chain lengths.

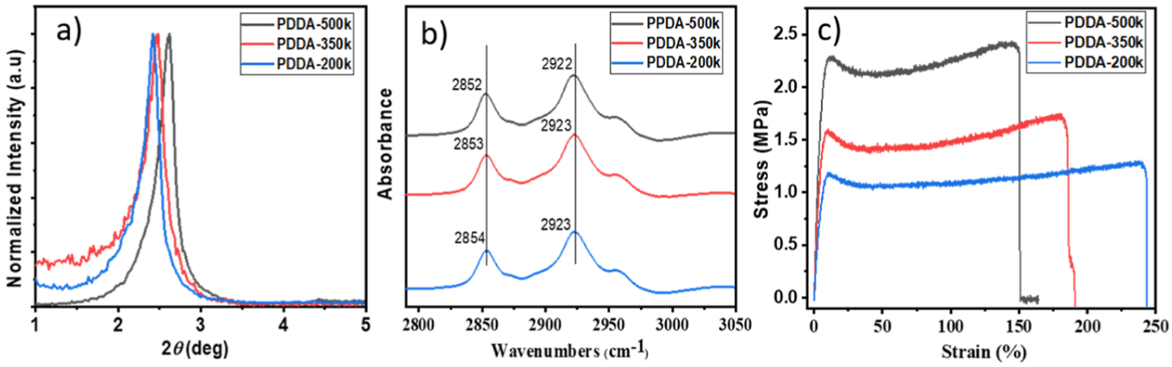

Figure 5. Effect of the molecular weight of PDDA on the structure and properties of the PDDA–SDS film. (a) XRD patterns. (b) FT-IR spectra for the PDDA-SDS films of different PDDA molecular weights. (c) Mechanical test for the PDDA–SDS films of different PDDA molecular weights.

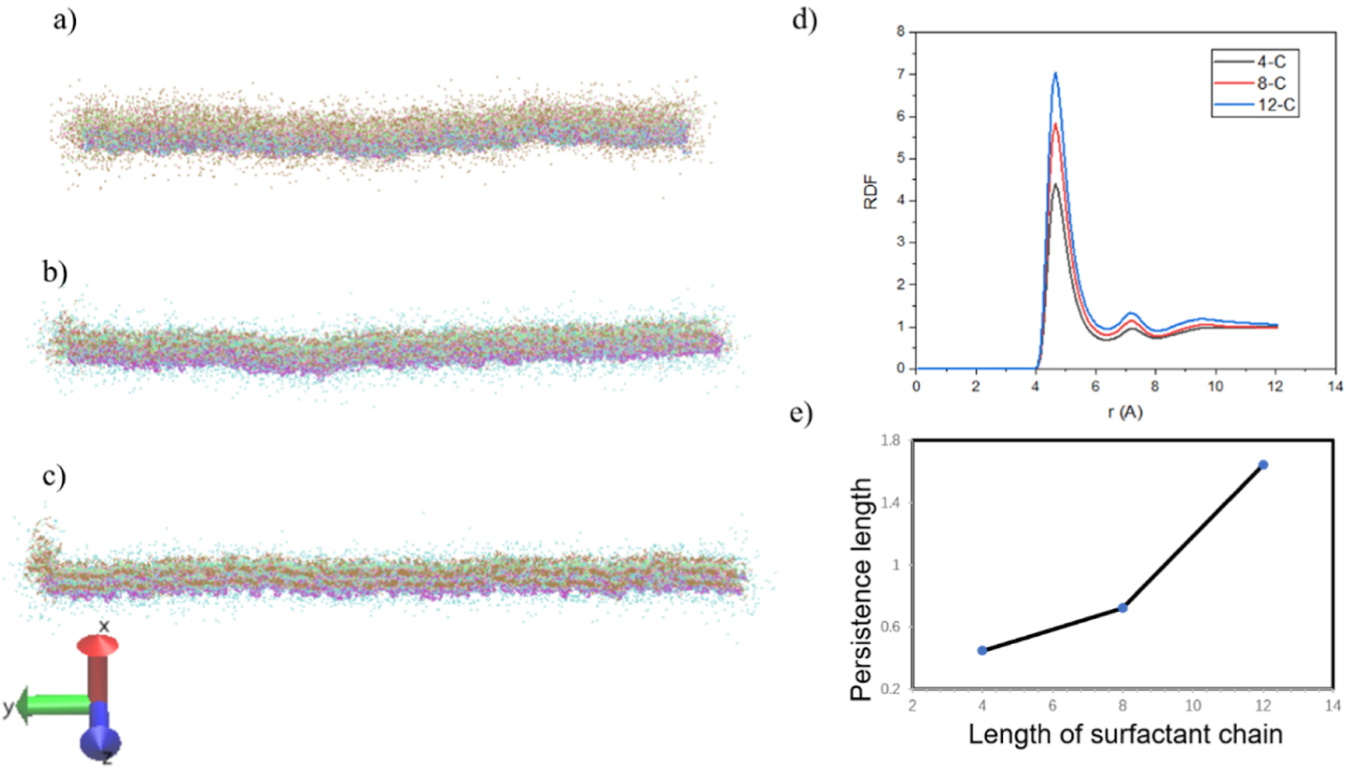

Figure 6. Last frame (5.0 ns) of SPMSA between PDDA and sodium alkyl sulfate visualized by VMD in the same scale for (a) SBS, (b) SOS, and (c) SDS. (d) RDF curves for different carbon chain lengths. (e) Graph depicting the relationship between alkyl sodium sulfate chain length and persistence length.

simplest structure of the PDDA polymer chain is shown in Figure 2d, and its relevant parameters are provided in Tables 1 and 3. In this context, the quaternary ammonium headgroup is denoted as "SN3q" for the two terminal groups and "SC3q" for the flexible chain structure with four beads located on the backbone. According to the force field file in Table 3, this cyclic structure is fixed, with the SC3q-SNq3q distance and SC3q-SC3q distance within a single monomer being set to 2.9948 and 2.2948 Å, respectively. Only relaxation of lengths and angles is allowed between the polymer units.

3.2.1. Simulation of the Effect of Surfactant Length on the SPMSA Structure. Based on the 5.0 ns simulation with a 10 fs time step, the last frame is given in Figure 6a−c, and the trajectories are given in Movie SV1 in the Supporting Information. The radial distribution functions (RDF) of the head groups of the surfactant of different chain lengths in the films were analyzed, and the results are shown in Figure 6d. The RDF curves exhibit higher peaks with increasing surfactant chain length, indicating a higher degree of ordering. Furthermore, the persistence length of the PDDA backbone in the films formed with these surfactants was analyzed using MDAnalysis.[50] Figure 6e shows that the persistence lengths of PDDA in the three films were found to be 0.447 nm for 4C, 0.721 nm for 8C, and 1.640 nm for 12C systems, respectively. This means that with increasing packing order of the surfactant in the film, the PDDA chains, which should lie on the surface of the surfactant bilayers, display stronger bridging ability between different surfactant bilayers. As a result, the strain at breaking should increase with increasing surfactant chain length. This is indeed the case observed in experiments. It is clear in Figure 4c that the mechanical strength for the PDDA-SDS and PDDA-SDeS films are nearly the same, but the breaking strains for the longer SDS system and short SDeS system are about 150 and 80%, respectively. Therefore, the increased packing order is advantageous for promoting the strain of the SPMSA films. The perfect agreement between the experimental and theoretical results unambiguously validates our CG-MD calculations in this work.

3.2.2. Simulation of the Molecular Weight of PDDA on the SPMSA Structure and Mechanical Strength. Next, we calculated the effect of the molecular weight of PDDA on the structure and mechanical strength of the films. In this case, the length of the surfactant chain remains 12, namely, fixing the surfactant to be SDS. The polymerization degree of the PDDA was independently adjusted, varying across four distinct values: 10, 100, 300, and 600. The simulation box is 180 nm × 180 nm × 1.5 nm. Following a 5 ns simulation with a 10 fs time step, the resulting membrane structures are schematically represented in Figure 7 and Movie SV2. The figure exclusively illustrates the configuration of the polymer backbone, omitting small molecules and water molecules from the depiction. Moreover, the potential energy change in 5 ns is given in Figure S1, where it can stabilize well within the range of 3−5 ns.

By examination of the trajectory plot, it becomes evident that the polymer backbones depicted in Figure 7a,b exhibit a more intricate configuration, with noticeable irregularities along their boundaries. However, at higher polymerization degrees of 300 (Figure 7c) and 600 (Figure 7d), remarkably neat and well-defined boundaries are formed. Based on ImageJ,[51] the Fourier transform image (the lower right corner of the big image in Figure 7) for each simulation was obtained. In the Fourier transform images, the fuzzy circle outside the center highlights the orientation state of the polymeric backbones. It is found that the simulation for the film formed with PDDA with a polymerization degree of 10 looks like a closed ring, indicating that all of the polymer chains do not take any orientation. This means the surfactant bilayers are not well bridged by the short PDDA chains to form large-sized structures. In contrast, as the polymerization degree of PDDA is greater than 100, the FFT images display two distinct spots symmetrically distributed around the circle center, manifesting the presence of oriented structures. Since the orientation of the PDDA should be induced by the surfactant bilayers in the SPMSA films, these FFT results indicate the presence of large oriented surfactant bilayers as the chain length (molecular weight) of PDDA increases. However, the current simulation may not provide information on the influence of various long chains of PDDA on the film's structure. It does, however, demonstrate that the length of the PE chain does have an impact on the degree of caking, which determines the size of the surfactant bilayers. This means that the physical insight for the ability of the longer PE chains in promoting the mechanical strength lies in two aspects: one is the formation of robust bridges between the surfactant bilayers and the other is to form large surfactant domains to enforce the films.

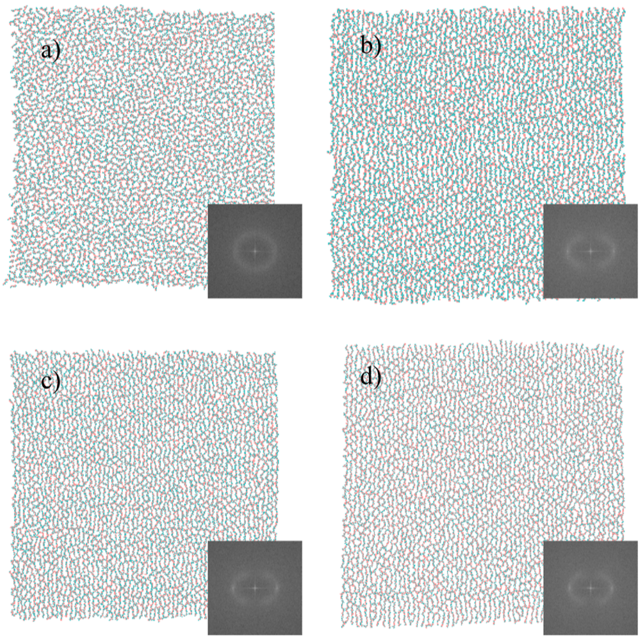

Figure 7. MD simulation results and the FFT reverse picture of SPMSA with the same surfactant SDS and varying the polymerization degree of PDDA. From (a) to (d), the polymerization degree of PDDA was set to be 10, 100, 300 and 600, respectively. The simulation box is 180 nm × 180 nm × 1.5 nm.

4. CONCLUSIONS

In the context of SPMSA involving surfactants and oppositely charged polyelectrolytes, a comprehensive multiscale CG-MD simulation was undertaken to understand the experimental results in terms of the interplay of alkyl chain length of surfactants and the degree of polymerization of the polyelectrolyte. The simulation findings suggest that increasing the alkyl chain length within a certain range favors and enhances the occurrence of solid-phase self-assembly. Consequently, a higher level of orderliness of molecules is achieved in the solid-phase self-assembled structures, which yields a higher mechanical strength. The CG-MD results also revealed that as the polymer chain length increases, the same surfactant chains would pack more orderly in the SPMSA. All these calculations are in perfect agreement with the experimental results. The current work shows that CG-MD calculation can be used to guide the creation of SPMSA materials and offers distinct physical insights into the interplay between the surfactant and PE.

■ ASSOCIATED CONTENT

Supporting Information

The Supporting Information is available free of charge at https://pubs.acs.org/doi/10.1021/acs.jpcb.3c07071.

Additional CG-MD results, including the potential energy change with time (PDF)

Two loops of 5 ns trajectories (MP4)

Resulting membrane structures following a 5 ns simulation with a 10fs time step (MP4)

■ AUTHOR INFORMATION

Corresponding Author

Yun Yan − *Beijing National Laboratory for Molecular Sciences (BNLMS), Beijing 100190, China; College of Chemistry and Molecular Engineering, Peking University, Beijing 100871, China;* orcid.org/0000-0001-8759-3918; Email: yunyan@pku.edu.cn

Authors

Xiangyu Dou − *Beijing National Laboratory for Molecular Sciences (BNLMS), Beijing 100190, China; College of Chemistry and Molecular Engineering, Peking University, Beijing 100871, China;* orcid.org/0000-0003-4219-5777

Shuitao Gao − *Beijing National Laboratory for Molecular Sciences (BNLMS), Beijing 100190, China; College of Chemistry and Molecular Engineering, Peking University, Beijing 100871, China*

Zekang Lu − *Beijing National Laboratory for Molecular Sciences (BNLMS), Beijing 100190, China; College of Chemistry and Molecular Engineering, Peking University, Beijing 100871, China*

Jianbin Huang − *Beijing National Laboratory for Molecular Sciences (BNLMS), Beijing 100190, China; College of Chemistry and Molecular Engineering, Peking University, Beijing 100871, China*

Complete contact information is available at: https://pubs.acs.org/10.1021/acs.jpcb.3c07071

Author Contributions

[§]X.D. and S.G. contributed equally.

Notes

The authors declare no competing financial interest.

■ ACKNOWLEDGMENTS

The authors are grateful to the National Natural Science Foundation of China (grants 22332001, 22172004, 21972003, 22202006) and the Beijing National Laboratory for Molecular Sciences (BNLMS) for financial support. The simulation work was supported by High-performance Computing Platform of Peking University. They also thank Professor Zhirong Liu of Peking University, Prof. Tao Chen of North West University, and Prof. Zhongyuan Lu of Jilin University, for their kindest help in setting CG models.

■ REFERENCES

(1) Ward, M. D.; Raithby, P. R. Functional behaviour from controlled self-assembly: challenges and prospects. *Chem. Soc. Rev.* **2013**, *42* (4), 1619−1636.

(2) Faul, C. F. J. Ionic Self-Assembly for Functional Hierarchical Nanostructured Materials. *Acc. Chem. Res.* **2014**, *47* (12), 3428−3438.

(3) Gao, S. T.; Qi, J. W.; Jiang, S. S.; Wu, T. Y.; Wang, W. K.; Cai, Y. T.; Ma, C.; Zhang, B.; Huang, J. B.; Yan, Y. Green wood adhesives from one-pot coacervation of folic acid and branched poly(ethylene imine). *ACS Appl. Bio Mater.* **2021**, *4* (9), 7314−7321.

(4) Li, J. L.; Yuan, S.; Qin, J. S.; Pang, J. D.; Zhang, P.; Zhang, Y. M.; Huang, Y. Y.; Drake, H. F.; Liu, W. R.; Zhou, H. C. Stepwise assembly of turn-on fluorescence sensors in multicomponent metal-organic frameworks for in vitro cyanide detection. *Angew. Chem., Int. Ed.* **2020**, *59* (24), 9319−9323.

(5) Yamanoi, Y.; Nakae, T.; Nishihara, H. Bio-organic-inorganichybrid soft materials: photoelectric conversion systems based on photosystem I and II with molecular wires. *Chem. Lett.* **2021**, *50* (6), 1263−1270.

(6) Chen, H. L.; Zhang, W. N.; Li, M. L.; He, G.; Guo, X. F. Interface engineering in organic field-effect transistors: principles, applications, and perspectives. *Chem. Rev.* **2020**, *120* (5), 2879−2949.

(7) Liao, P. L.; Huang, J. B.; Yan, Y.; Tang, B. Z. Clusterization-triggered emission (CTE): one for all, all for one. *Mater. Chem. Front.* **2021**, *5* (18), 6693−6717.

(8) Qi, W. L.; Wang, X. J.; Liu, Z. Y.; Liu, K. E. D.; Long, Y. F.; Zhi, W. W.; Ma, C.; Yan, Y.; Huang, J. B. Visual recognition of ortho-xylene based on its host-guest crystalline self-assembly with α-cyclodextrin. *J. Colloid Interface Sci.* **2021**, *597*, 325−333.

(9) Gorl, D.; Zhang, X.; Stepanenko, V.; Wurthner, F. Supramolecular block copolymers by kinetically controlled co-self-assembly of planar and core-twisted perylene bisimides. *Nat. Commun.* **2015**, *6*, 7009.

(10) Liu, T. B. Hydrophilic macroionic solutions: what happens when soluble ions reach the size of nanometer scale? *Langmuir* **2010**, *26* (12), 9202−9213.

(11) Escobar, L.; Ballester, P. Molecular recognition in water using macrocyclic synthetic receptors. *Chem. Rev.* **2021**, *121* (4), 2445−2514.

(12) Kumar, R.; Sharma, A.; Singh, H.; Suating, P.; Kim, H. S.; Sunwoo, K.; Shim, I.; Gibb, B. C.; Kim, J. S. Revisiting fluorescent calixarenes: from molecular sensors to smart materials. *Chem. Rev.* **2019**, *119* (16), 9657−9721.

(13) Liu, T. B.; Langston, M. L. K.; Li, D.; Pigga, J. M.; Pichon, C.; Todea, A. M.; Muller, A. Self-recognition among different polyprotic macroions during assembly processes in dilute solution. *Science* **2011**, *331* (6024), 1590−1592.

(14) Han, L.; Yan, L. W.; Wang, M. H.; Wang, K. F.; Fang, L. M.; Zhou, J.; Fang, J.; Ren, F. Z.; Lu, X. Transparent, Adhesive, and Conductive Hydrogel for Soft Bioelectronics Based on Light-Transmitting Polydopamine-Doped Polypyrrole Nanofibrils. *Chem. Mater.* **2018**, *30* (16), 5561−5572.

(15) Zhao, T. H.; Han, J. L.; Jin, X.; Liu, Y.; Liu, M. H.; Duan, P. F. Enhanced Circularly Polarized Luminescence from Reorganized Chiral Emitters on the Skeleton of a Zeolitic Imidazolate Framework. *Angew. Chem., Int. Ed.* **2019**, *58* (15), 4978−4982.

(16) Zhao, Z. G.; Li, C. X.; Dong, Z. C.; Yang, Y. C.; Zhang, L. H.; Zhuo, S. Y.; Zhou, X. T.; Xu, Y. C.; Jiang, L.; Liu, M. J. Adaptive Superamphiphilic Organohydrogels with Reconfigurable Surface Topography for Programming Unidirectional Liquid Transport. *Adv. Funct. Mater.* **2019**, *29* (16), 1807858.

(17) Wang, Y.; Li, T. Q.; Li, S. H.; Guo, R. B.; Sun, J. Q. Healable and Optically Transparent Polymeric Films Capable of Being Erased on Demand. *ACS Appl. Mater. Interfaces* **2015**, *7* (24), 13597−13603.

(18) An, N.; Wang, X. H.; Li, Y. X.; Zhang, L.; Lu, Z. Y.; Sun, J. Q. Healable and Mechanically Super-Strong Polymeric Composites Derived from Hydrogen-Bonded Polymeric Complexes. *Adv. Mater.* **2019**, *31* (41), 1904882.

(19) Lunn, D. J.; Gould, O. E. C.; Whittell, G. R.; Armstrong, D. P.; Mineart, K. P.; Winnik, M. A.; Spontak, R. J.; Pringle, P. G.; Manners, I. Microfibres and macroscopic films from the coordination-driven hierarchical self-assembly of cylindrical micelles. *Nat. Commun.* **2016**, *7*, 12371.

(20) Niu, W. W.; Zhu, Y. L.; Wang, R.; Lu, Z. Y.; Liu, X. K.; Sun, J. Q. Remalleable, healable, and highly sustainable supramolecular polymeric materials combining superhigh strength and ultrahigh toughness. *ACS Appl. Mater. Interfaces* **2020**, *12* (27), 30805−30814.

(21) Zafar, U.; Vivacqua, V.; Calvert, G.; Ghadiri, M.; Cleaver, J. A. S. A review of bulk powder caking. *Powder Technol.* **2017**, *313*, 389−401.

(22) Carpin, M.; Bertelsen, H.; Bech, J. K.; Jeantet, R.; Risbo, J.; Schuck, P. Caking of lactose: A critical review. *Trends Food Sci. Technol.* **2016**, *53*, 1−12.

(23) Wang, W. K.; Xie, M. Q.; Jin, H. J.; Zhi, W. W.; Liu, K.; Ma, C.; Liao, P. L.; Huang, J. B.; Yan, Y. The pressing-induced formation of a large-area supramolecular film for oil capture. *Mater. Chem. Front.* **2020**, *4* (5), 1530−1539.

(24) Jin, H. J.; Xie, M. Q.; Wang, W. K.; Jiang, L. X.; Chang, W. Y.; Sun, Y.; Xu, L. M.; Zang, S. H.; Huang, J. B.; Yan, Y.; et al. Pressing-induced caking: a general strategy to scale-span molecular self-assembly. *CCS Chem.* **2020**, *2* (2), 98−106.

(25) Xie, M. Q.; Che, Y. X.; Liu, K.; Jiang, L. X.; Xu, L. M.; Xue, R. R.; Drechsler, M.; Huang, J. B.; Tang, B. Z.; Yan, Y. Caking-Inspired Cold Sintering of Plastic Supramolecular Films as Multifunctional Platforms. *Adv. Funct. Mater.* **2018**, *28* (36), 1803370.

(26) Wu, T. Y.; Gao, S. T.; Wang, W. K.; Huang, J. B.; Yan, Y. Wearable Sensors Based on Solid-Phase Molecular Self-Assembly: Moisture-Strain Dual Responsiveness Facilitated Extremely High and Damage-Resistant Sensitivity. *ACS Appl. Mater. Interfaces* **2021**, *13* (35), 41997−42004.

(27) Jin, H.; Ma, C.; Wang, W.; Cai, Y.; Qi, J.; Wu, T.; Liao, P.; Li, H.; Zeng, Q.; Xie, M.; et al. Using molecules with superior water-plasticity to build solid-phase molecular self-assembly: room-temperature engineering mendable and recyclable functional supramolecular plastics. *ACS Mater. Lett.* **2022**, *4* (1), 145−152.

(28) Liao, P. L.; Zang, S. H.; Wu, T. Y.; Jin, H. J.; Wang, W. K.; Huang, J. B.; Tang, B. Z.; Yan, Y. Generating circularly polarized luminescence from clusterization-triggered emission using solid phase molecular self-assembly. *Nat. Commun.* **2021**, *12* (1), 5496.

(29) Qi, J.; Wu, T.; Wang, W.; Jin, H.; Gao, S.; Jiang, S.; Huang, J.; Yan, Y. Solid-phase molecular self-assembly facilitated supramolecular films with alternative hydrophobic/hydrophilic domains for skin moisture detection. *Aggregate* **2022**, *3* (2), No. e173.

(30) Wu, T.; Guo, J.; Huang, J.; Yan, Y. Robust single molecular white fluorescence facilitated by blocking aggregate growth in Densely-Woven solid polymeric network. *Chem. Eng. J.* **2023**, *457*, 140974.

(31) Jin, H.; Cai, Y.; Li, H.; Liao, P.; Wu, T.; Ma, C.; Chen, Q.; Qian, Q.; Huang, J.; Yan, Y. Photo-Enhanced-Coordination Triggered Unprecedented Bistable AIE for Long-Term Optical Memories. *Adv. Opt. Mater.* **2022**, *10* (11), 2200130.

(32) Jin, H.; Lin, W.; Wu, Z.; Cheng, X.; Chen, X.; Fan, Y.; Xiao, W.; Huang, J.; Qian, Q.; Chen, Q.; et al. Surface Hydrophobization Provides Hygroscopic Supramolecular Plastics Based on Polysaccharides with Damage-Specific Healability and Room-Temperature Recyclability. *Adv. Mater.* **2023**, *35* (8), 2207688.

(33) Jin, H.; Li, H.; Zhu, Z.; Huang, J.; Xiao, Y.; Yan, Y. Hydration-Facilitated Fine-Tuning of the AIE Amphiphile Color and Application as Erasable Materials with Hot/Cold Dual Writing Modes. *Angew. Chem., Int. Ed.* **2020**, *59* (25), 10081−10086.

(34) Wang, W.; Song, H.; Lu, Z.; Zeng, Q.; Wang, Q.; Ma, C.; Jin, H.; Qi, J.; Wu, T.; Gao, S.; et al. Mussel Byssus Inspired Ionic Skin with Damage-Resistant Signal for Human-Machine Interaction. *Adv. Mater. Interfaces* **2022**, *9* (34), 2201367.

(35) Jin, H. J.; Ma, C.; Wang, W. K.; Cai, Y. T.; Qi, J. W.; Wu, T. Y.; Liao, P. L.; Li, H. P.; Zeng, Q.; Xie, M. Q.; et al. Using molecules with superior water-plasticity to build solid-phase molecular self-assembly: room-temperature engineering mendable and recyclable functional supramolecular plastics. *ACS Mater. Lett.* **2022**, *4*, 145−152.

(36) Dou, X. Y.; Jin, H. J.; Wu, T. Y.; Huang, J. B.; Zhang, B.; Liu, Z. R.; Chen, T.; Yan, Y. Physical Insight into the Conditions Required in the Solid-Phase Molecular Self-Assembly of SDS Revealed by Coarse-Grained Molecular Dynamics Simulation. *J. Phys. Chem. B* **2022**, *126* (33), 6345−6353.

(37) Dodda, L. S.; Vilseck, J. Z.; Tirado-Rives, J.; Jorgensen, W. L. 1.14*CM1A-LBCC: localized bond-charge corrected CM1A charges for condensed-phase simulations. *J. Phys. Chem. B* **2017**, *121* (15), 3864−3870.

(38) Dodda, L. S.; Cabeza de Vaca, I.; Tirado-Rives, J.; Jorgensen, W. L. LigParGen web server: an automatic OPLS-AA parameter generator for organic ligands. *Nucleic Acids Res.* **2017**, *45* (W1), W331−W336.

(39) Souza, P. C. T.; Alessandri, R.; Barnoud, J.; Thallmair, S.; Faustino, I.; Grunewald, F.; Patmanidis, I.; Abdizadeh, H.; Bruininks, B. M. H.; Wassenaar, T. A.; et al. Martini 3: a general purpose force field for coarse-grained molecular dynamics. *Nat. Methods* **2021**, *18* (4), 382−388.

(40) Harder, E.; Damm, W.; Maple, J.; Wu, C.; Reboul, M.; Xiang, J. Y.; Wang, L.; Lupyan, D.; Dahlgren, M. K.; Knight, J. L.; et al. OPLS3: a force field providing broad coverage of drug-like small molecules and proteins. *J. Chem. Theory Comput.* **2016**, *12* (1), 281−296.

(41) Kahn, K.; Bruice, T. C. Parameterization of OPLS-AA force field for the conformational analysis of macrocyclic polyketides. *J. Comput. Chem.* **2002**, *23* (10), 977−996.

(42) Souza, P. C. T.; Alessandri, R.; Barnoud, J.; Thallmair, S.; Faustino, I.; Grünewald, F.; Patmanidis, I.; Abdizadeh, H.; Bruininks, B. M. H.; Wassenaar, T. A.; et al. Martini 3: a general purpose force field for coarse-grained molecular dynamics. *Nat. Methods* **2021**, *18* (4), 382−388.

(43) Damm, W.; Frontera, A.; TiradoRives, J.; Jorgensen, W. L. OPLS all-atom force field for carbohydrates. *J. Comput. Chem.* **1997**, *18* (16), 1955−1970.

(44) Jorgensen, W. L.; Maxwell, D. S.; TiradoRives, J. Development and testing of the OPLS all-atom force field on conformational energetics and properties of organic liquids. *J. Am. Chem. Soc.* **1996**, *118* (45), 11225−11236.

(45) Marrink, S. J.; Risselada, H. J.; Yefimov, S.; Tieleman, D. P.; de Vries, A. H. The MARTINI force field: coarse grained model for biomolecular simulations. *J. Phys. Chem. B* **2007**, *111* (27), 7812−7824.

(46) Wang, S. H.; Larson, R. G. Coarse-Grained Molecular Dynamics Simulation of Self-Assembly and Surface Adsorption of Ionic Surfactants Using an Implicit Water Model. *Langmuir* **2015**, *31* (4), 1262−1271.

(47) Yan, Y.; Xiong, W.; Huang, J.; Li, Z.; Li, X.; Li, N.; Fu, H. Organized Assemblies in Bolaamphiphile/Oppositely Charged Conventional Surfactant Mixed Systems. *J. Phys. Chem. B* **2005**, *109* (1), 357−364.

(48) Yan, Y.; Hoffmann, H.; Makarsky, A.; Richter, W.; Talmon, Y. Swelling of L_α-Phases by Matching the Refractive Index of the Water−Glycerol Mixed Solvent and that of the Bilayers in the Block Copolymer System of $(EO)_{15}-(PDMS)_{15}-(EO)_{15}$. *J. Phys. Chem. B* **2007**, *111* (23), 6374−6382.

(49) Jiang, L.; Peng, Y.; Yan, Y.; Huang, J. Aqueous self-assembly of SDS@2β-CD complexes: lamellae and vesicles. *Soft Matter* **2011**, *7* (5), 1726−1731.

(50) Michaud-Agrawal, N.; Denning, E. J.; Woolf, T. B.; Beckstein, O. MDAnalysis: A toolkit for the analysis of molecular dynamics simulations. *J. Comput. Chem.* **2011**, *32* (10), 2319−2327.

(51) Schneider, C. A.; Rasband, W. S.; Eliceiri, K. W. NIH Image to ImageJ: 25 years of image analysis. *Nat. Methods* **2012**, *9* (7), 671−675.